Available online at www.sciencedirect.com
SCIENCE DIRECT®
Journal of Power Sources 136 (2004) 250–256
JOURNAL OF POWER SOURCES
www.elsevier.com/locate/jpowsour

High voltage electrochemical double layer capacitors using conductive carbons as additives

M.S. Michael, S.R.S. Prabaharan*

Center for Smart Systems and Innovation, Advanced Power Sources Laboratory, Faculty of Engineering, Multimedia University, 63100 Cyberjaya, Malaysia

Abstract

We describe here an interesting approach towards electrochemical capacitors (ECCs) using graphite materials (as being used as conductive additives in rechargeable lithium-ion battery cathodes) in a Li^+ containing organic electrolyte. The important result is that we achieved a voltage window of >4 V, which is rather large, compared to the standard window of 2.5 V for ordinary electric double layer capacitors (DLCs). The capacitor performance was evaluated by cyclic voltammetry (CV) and galvanostatic charge/discharge techniques. From charge–discharge studies of the symmetrical device (for instance, SFG6 carbon electrode), a specific capacitance of up to 14.5 F/g was obtained at 16 mA/cm^2 current rate and at a low current rate (3 mA/cm^2), a higher value was obtained (63 F/g). The specific capacitance decreased about 25% after 1000 cycles compared to the initial discharge process. The performances of these graphites are discussed in the light of both double layer capacitance (DLC) and pseudocapacitance (battery-like behavior). The high capacitance obtained was not only derived from the current-transient capacitive behavior but is also attributed to pseudocapacitance associated with some kind of faradaic reaction, which could probably occur due to Li^+ intercalation/deintercalation reactions into graphitic layers of the carbons used. The ac impedance (electrochemical impedances spectroscopy, EIS) measurements were also carried out to evaluate the capacitor parameters such as equivalent series resistance (ESR) and frequency dependent capacitance (C_{freq}). Cyclic voltammetry measurements were also performed to evaluate the cycling behavior of the carbon electrodes and the non-rectangular shaped voltammograms revealed the non-zero time constant [$\tau(RC) \neq 0$] confirming that the current contains a transient as well as steady-state components.

Keywords: Electrochemical capacitors; Double layer capacitors; Pseudo capacitors; Conductive additive carbons; Organic electrolytes; Ragone plot

1. Introduction

Batteries and capacitors are regarded as traditional electrical energy storage devices. Batteries deliver high-energy density but limited power output and therefore they are suitable for applications requiring energy delivery over extended periods. In contrast, capacitors, which can deliver their energy at high rate, can only do so for a limited time. This has led to the intense investigation of a new type of energy storage devices known as electrochemical capacitors (ECCs), also called ultra- or supercapacitors [1,2]. No phase changes are involved in the electrochemical processes of ECCs, and therefore, they can be charged and discharged many times. ECCs have many potential applications, ranging from load leveling devices for electric vehicles to pulse power sources for hand held electronics [3]. Thus, an ECC can combine the energy storage capability of a battery and power storage behavior of normal capacitors and fill the gap between high-powered normal capacitors and high-energy batteries [4,5].

Two types of ECCs have enjoyed extensive development over the last decades. Double layer capacitors (DLCs) were considered first [6], and consist of porous electrodes in an electrolyte solution that store charge in the electrochemical double layer formed at the electrode/electrolyte solution interface when a potential is applied. Since, the typical double layer capacitance of a planar electrode is only 10–20 μF/cm^2 [7], high surface area materials like activated carbons (>1000 m^2/g) are employed.

DLCs can be used as pulse power sources for digital communication devices and hybrid electric vehicles (HEVs). Recently, the hybrid power source that consists of electrochemical capacitors in parallel with a battery bank was proposed for electric vehicle propulsion in which the latter performs as a high-energy device while the former supplies high power.

The second type of ECC is based on the pseudocapacitance observed with materials such as noble metal

* Corresponding author. Tel.: +60-3-8312-5378; fax: +60-3-8318-3029.
E-mail address: prabaharan@mmu.edu.my (S.R.S. Prabaharan).

0378-7753/$ – see front matter © 2004 Elsevier B.V. All rights reserved.
doi:10.1016/j.jpowsour.2004.03.006

oxides (RuO_2 and IrO_2) or conducting polymers [8–10]. In such devices, the charge transfer involves faradaic redox reactions. Devices utilizing this method of charge storage can provide higher energy and power density than DLCs since the charge is stored throughout the bulk of the materials as well as at the electrode/electrolyte interface [11].

Conway et al., discussed the transition from "supercapacitor" to "battery behavior" in electrochemical energy storage and the origin of "pseudo-capacitor" [12], which could be considered as "capacitor behavior".

The limitation of ECCs is the low cell voltage, which is determined by the decomposition of the aqueous electrolytes. Thus, the maximum voltage attainable in ECC using aqueous electrolyte is restricted to ~1.0 V. However, the cell voltage of an ECC can be increased above 3.0 V by replacing aqueous electrolyte with organic nonaqueous electrolyte [13]. Increasing the voltage of an ECC enhances the specific energy of the capacitor device, as the ECCs are known for specific power. Besides, when ECCs are used in hybrid combination with high voltage rechargeable batteries so as to meet the requirement that voltage of both battery and capacitor should be equal in charged state, four to five capacitors have to be connected in series. In other words, fewer capacitors are enough when the voltage of ECC is high. In this context, the present study focuses on the enhancement in voltage using the chosen carbons (graphite) being used as conductive additives in the electrodes of rechargeable Li-ion batteries. Nowadays, nonaqueous electrolytes with a high potential window (>4.5 V) are commercially available for Li-ion battery applications. However, the high specific resistance of nonaqueous electrolytes considerably increases the equivalent series resistance (ESR) as well as diminishing the overall capacitance by a factor of two or less which results in a lowering of power density. On the other hand, high working voltage of ECC using organic electrolyte enhances the energy density in excess of a three-fold. As a consequence, the electrochemical capacitors using organic electrolytes are very much used when high-energy density and modest power density is desirable.

To achieve the outstanding capacitance of ECCs, porous carbon (for instance activated carbons) with very high surface area (>1500 m^2/g) were used [14–19]. However, the use of organic electrolytes in ECCs to achieve high voltage might lead to corrosion of carbon electrodes at high voltage and the rate of such corrosion increases due to the porosity (pore distribution). In order to diminish such high voltage corrosion on carbon electrodes, surface modification methods were recently described [20]. Ue et al. [6], studied the suitability of different organic electrolytes for supercapacitors and found that tetra ethyl ammonium tetra fluoroborate ($TEABF_4$) in acetonitrile is the best one, with a floating voltage of 2.6 V.

The rationale for choice of conductive additive carbons used in this work as electrodes for ECCs is mainly due to profound compatibility of these carbons with highly oxidizing organic electrolytes and their stability at high voltages in lithium rechargeable batteries [21,22].

In the present study, ECCs of high voltage (4.5 V) were studied, employing conductive additive carbon electrodes and we have attempted to explain the origin of the measured high capacitance in the light of both DLC and pseudocapacitance concepts.

2. Experimental

Timrex® grade graphites namely KS6 (21 m^2/g), SFG6 (17 m^2/g), and MB15 (10 m^2/g) were provided by TIMCAL Co. Ltd. (Switzerland) and used as received. The desired quantities of carbon powders were made into a slurry by mixing with special PVDF binder (provided by Elf Atochem, France) in the 80:20 w/o ratio (carbon: binder) using THF (Merck, Germany). The slurry thus prepared was coated onto expanded aluminum mesh (Exmet, USA) as positive and negative electrode. The coating was allowed to dry at 80 °C for 30 min in a vacuum oven. The thickness of as-prepared coatings was controlled within 150 μm and the mass of the carbon material was maintained as 0.005–0.01 g/cm^2. Circular disks of area 3.14 cm^2 were cut from the coated mesh, soaked in the electrolyte mixture 1 M $LiPF_6$ in EC + DMC (LP30, Merck, Germany) for 30 min. A two-electrode Teflon cell with a coin cell (2450) configuration was used to assemble the cells inside a glove box filled with high purity argon. Electrode combinations such as similar and dissimilar carbon disk electrodes were sandwiched between 2400 Celgard® membranes. The total thickness of the capacitor was 0.5 mm excluding the housing. Microstructure and morphology information was obtained on graphite powders by SEM using a JEOL JSM 800 scanning electron microscope (SEM) interfaced with a personal computer through JEOL software.

The performance of ECC was evaluated and monitored by means of electrochemical techniques namely, galvanostatic charge/discharge and cyclic voltammetry (CV) by employing multichannel BT2000 Arbin testing system (USA). The electrochemical impedances spectroscopy (EIS) measurements were carried out by employing basic electrochemical system (PAR, Perkin-Elmer, and USA) equipped with power sine software. A constant DC bias of 0 V and ac perturbation of 10 mV (rms) was applied to the cells. The frequency was varied between 20 kHz and 5 mHz.

3. Results and discussion

3.1. Morphological study

SEM studies were carried out on the chosen conductive additive carbons such as SFG6, MB15, and KS6. Fig. 1 shows the electron micrographs obtained for the above

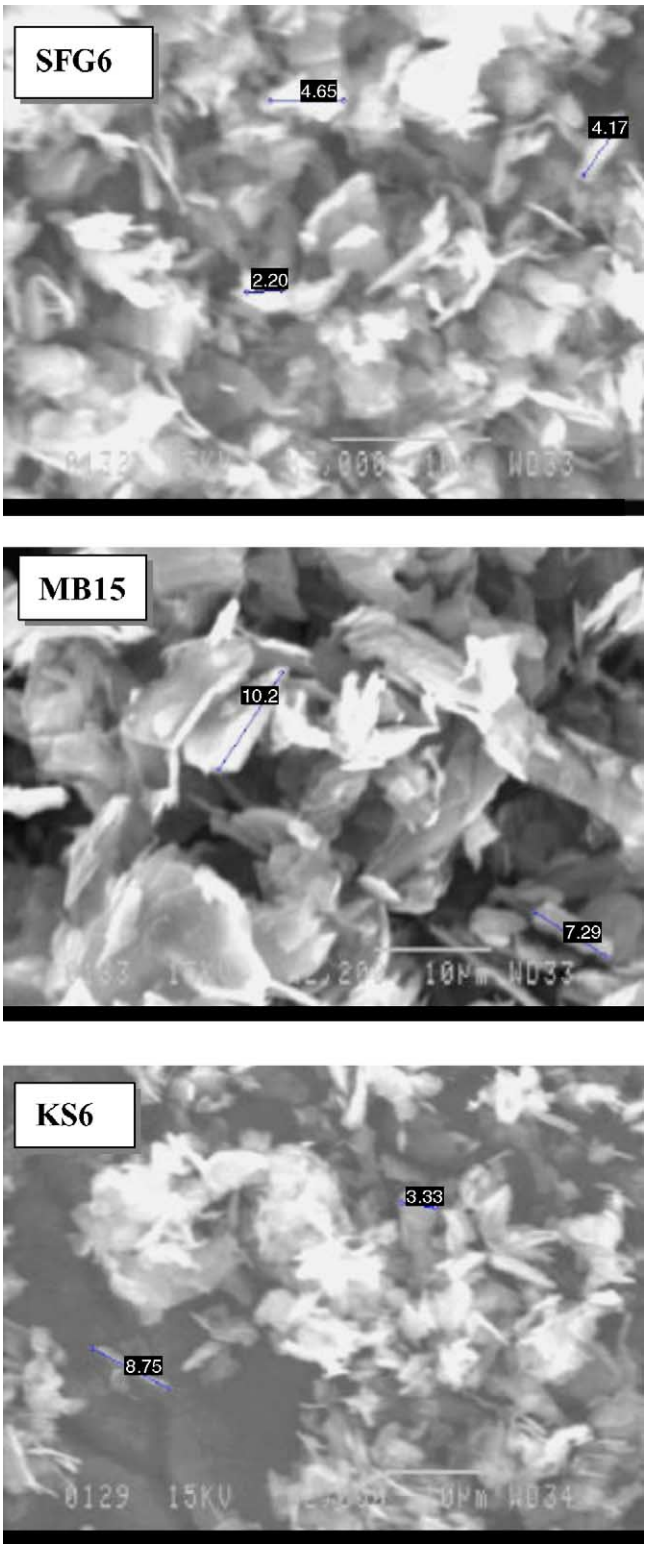

Fig. 1. SEM images of the conductive graphite additives showing the flakes with distributed grain sizes.

graphite powders and they all exhibit flake-like structure with sharp edges. Graphite KS 6 consists of fine particles compared to MB15 and SFG6. Invariably, the pore distribution is not explicitly seen from the micrographs, ruling out

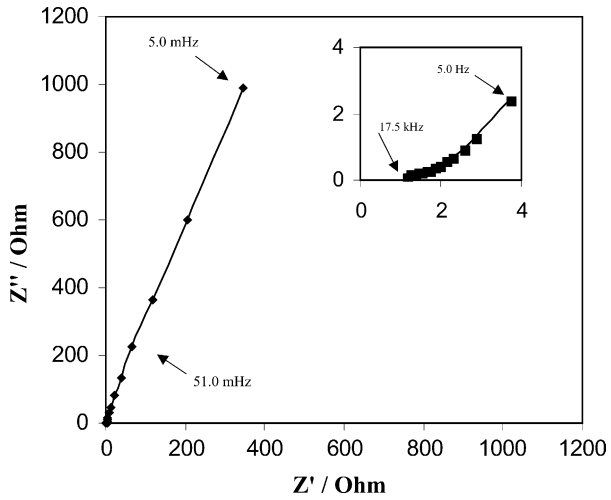

Fig. 2. Nyquist plot of a symmetrical device assembled with two similar electrodes (SFG6/SFG6) between the ac frequency range, 17.5 kHz up to 5 mHz; ac perturbation applied was 10 mV ESR values were measured at 1 kHz.

the possibility of having the porous structure of the above graphite electrodes.

3.2. Electrochemical impedances spectroscopy measurements

Fig. 2 presents the impedance response of a typical symmetrical device assembled with two similar electrodes (SFG6) employing 1 M $LiPF_6$/EC + DMC nonaqueous electrolyte. In general, ECCs oscillate between two states: resistance at high frequencies and capacitance at low frequencies. As shown in Fig. 2, the above behavior is clearly evident. That is, at high frequencies (17.5 kHz), it behaves like a resistance exhibiting the charge-transfer (R_{ct}) resistance and the imaginary part of the impedance sharply increases and the plot tends to a straight-line (a spike) characteristic of capacitive (DLC) behavior. In the middle frequency range, as shown in the inset of Fig. 2, the influence of electrode porosity and thickness on the migration rate of ions from the electrolyte inside the electrode (intercalation of Li^+) can be seen [23]. In this case, R_{ct} was found to be very small, followed by diffusional Warburg impedance (see inset) indicating the diffusion of ions into carbon layers, which could possibly be related to intercalation of Li^+ into graphitic layer leading to faradaic reaction.

The straight-line portion shows an inclination from the ideal capacitive behavior (vertical line) indicating the surface roughness of the electrodes. ESR values were deduced at 1 kHz real impedance data and were found to be 0.97 Ω for SFG6/SFG6 symmetrical device.

A symmetrical device assembled with MB15 graphite showed a lower ESR value of 1.31 Ω presumably due to the low electrode resistance.

Generally, the imaginary part of the ac impedance is converted to capacitance at a given frequency using the rela-

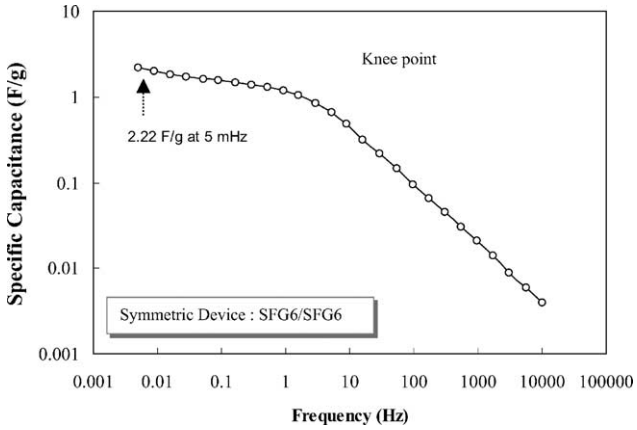

Fig. 3. Typical frequency dependence of specific capacitance of a SFG6/SFG6 symmetrical device.

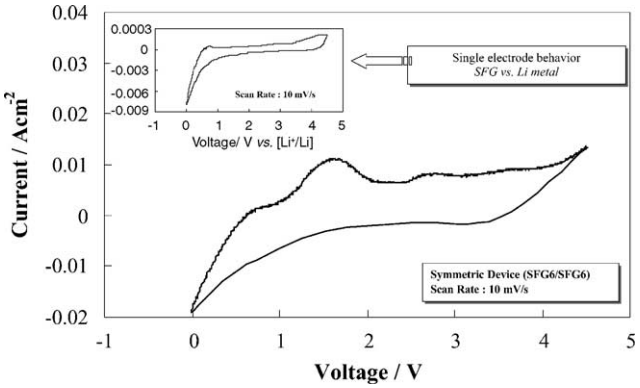

Fig. 4. Cyclic voltammetry of symmetrical device (SFG/SFG) in 1 M LiPF6/EC + DMC organic electrolyte (Celgard 2400 separator was used between the two carbon electrodes constituting the symmetrical electrode combination); scan rate was 10 mV/s. Inset shows the single electrode behavior against lithium metal in the same electrolyte using Celgard 2400 separator.

tionship, $Z''(\omega) = -1/\omega C$, where Z'' is the imaginary part of the impedance, ω is the angular frequency, and C is the capacitance (frequency dependent). In explaining the behavior of frequency dependence of capacitance, generally a two-slope region is expected for electrochemical capacitors where the capacitance increases noticeably towards low frequencies with increasing slope values from its high frequency counterpart.

Fig. 3 presents the specific capacitance versus frequency of the symmetrical device assembled with two electrodes (SFG6). It is clearly evident that frequency dependent capacitance exhibits two increasing slope regions; the first one occurs between high frequency (17.5 kHz) and ~5 Hz and the second region extended up to 5 mHz from the knee point. The two-slope behavior is much expected as described in the literature [24] that when the frequency decreases, capacitance sharply increases then lends to be less frequency dependent which is characteristic of the electrode structure and the electrode/electrolyte interface.

3.3. Voltammetry measurements

Potential sweep cyclic voltammetry measurements were carried out within the potential range of 0–4.5 V to analyze the electrochemical behavior of the capacitors.

Fig. 4 exhibits the typical voltammograms obtained for symmetrical device assembled with two similar electrodes (SFG6). The voltammogram is characterized by a few humps in the anodic half-cycle and the value of current is high. This effect was prominent for the device assembled with SFG6 graphite as shown in Fig. 4. In general, the equivalent circuit for DLC electrodes can be represented by a serial combination of equivalent series resistance and double layer capacitance [25]. If the faradaic reaction exists in the device, the equivalent circuit may be represented by an interfacial capacitance (C_{dl}) with ESR and parallel faradaic leakage resistance coupled with diffusional impedance (Warburg impedance) [24]. The shape of the voltammogram was duly determined by the time constant, $\tau(RC)$ of the device where R is the ESR and C is the device capacitance. The non-rectangular current–voltage profile revealed the non-zero time constant [$\tau(RC) \neq 0$] that indicates the current contains a transient part as well as a steady-state part. As τ becomes larger, the transient part lasts longer and hence more time is required to charge the capacitor resulting in a collapse of the rectangular current profile [26]. The shape of the voltammogram is also affected by a faradaic reaction (pseudocapacitance). Interestingly, it is evident from Fig. 4 that during the anodic scan, the anodic current rises to a peak maximum at 1.6 V with the onset begins at 0.7 V which is related to the charge-transfer reaction associated with the intercalation of Li^+. To confirm the above phenomenon, we studied the CV of a single electrode behavior against lithium metal to ascertain whether or not the faradaic process is due to Li^+ insertion/deinsertion process as depicted in Fig. 4 (see inset). We observed the quite similar behavior for other two graphites, MB 15 and KS 6 (not shown).

3.4. Constant current measurements (charge/discharge)

A typical galvanostatic first charge/discharge curves of symmetrical device electrode (SFG6/SFG6 combination) between the voltage range 0–4.5 V at a current density of 6 mA/cm^2 is shown in the Fig. 5. In the present case, since the maximum voltage of ECC is generally determined by the oxidation potential of the electrolyte, it is kept at 4.5 V as the upper cutoff voltage limit during charge. In general, the discharge profile of ECC contains two parts; a resistive component, a sudden voltage drop (iR drop) represents the voltage change due to the internal resistance of ECC and the capacitive component is related to the voltage change due to change in energy within the capacitor. The pattern is same irrespective of the type of graphite materials as well as the current density being used. Nevertheless, iR drop is large at higher current density because of the domination of

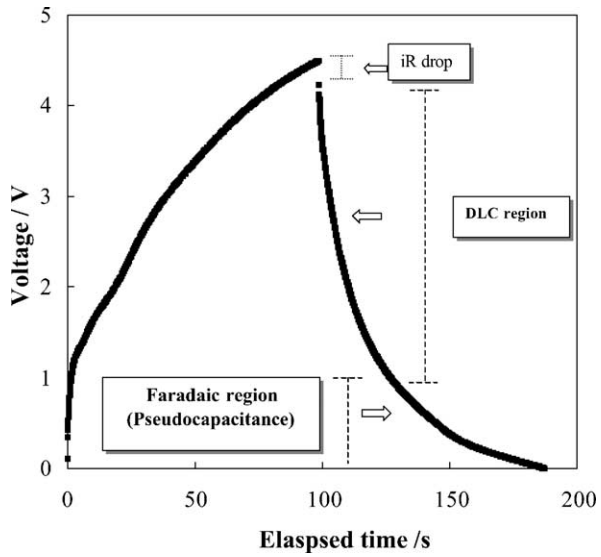

Fig. 5. Typical first charge/discharge curve of a symmetrical device capacitor (SFG6/SFG6) at a current rate of 6 mA/cm^2.

a resistive component while at a low current density, due to the domination of a capacitive component, the length of linear portion is large. Fig. 6 depicts the discharge curves of a symmetrical device, SFG6/SFG6, at different current rates and the inset clearly exhibits the *iR* drop influenced by the current rates in determining the performance of the capacitor and hence its specific capacitance. In this case, it was found that *iR* drop is 0.13 V, corresponding to a current density of 3 mA/cm^2 in which the linear portion (DL capacitance) extends for almost 100 S whereas it lasts for only 20 s at 16 mA/cm^2 current rate with an *iR* drop of 0.63 V. Besides, it was found that *iR* drop depends on the resistance of the graphite materials as well. It was also found that *iR* drop is lower for ECC using SFG6 while it is higher for MB15. This

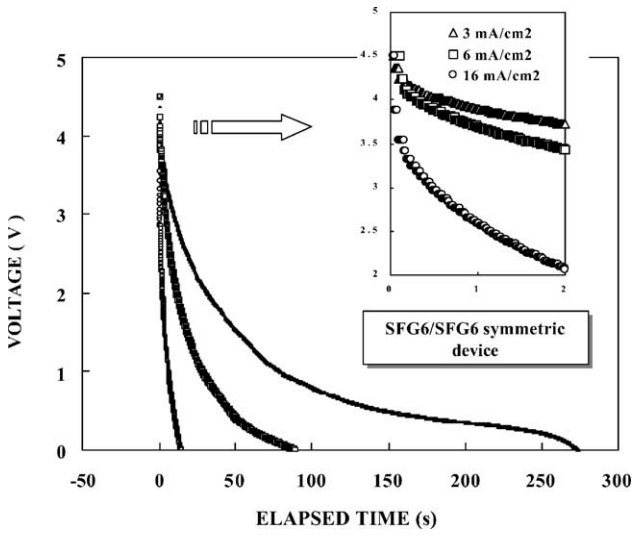

Fig. 6. Typical discharge curves of a SFG6/SFG6 capacitor at different discharge rates. (Expanded view of iR drop with respect to discharge current rate is depicted in the inset.)

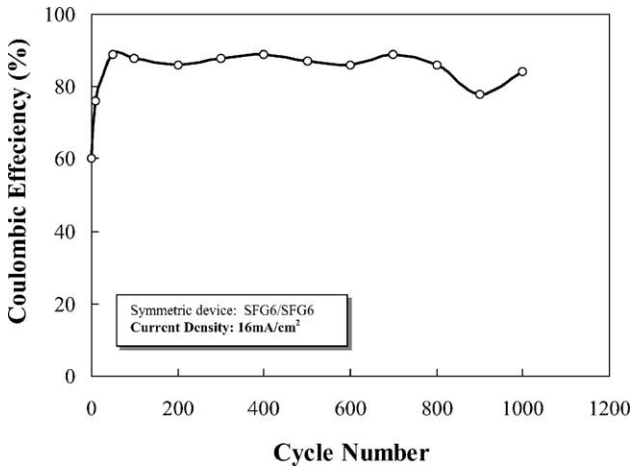

Fig. 7. Coulombic efficiency of a symmetrical device (SFG/SFG) as a function of cycle number.

might be due to higher electrode resistance ($R_{electrode}$) of the latter. When compared to ECCs with aqueous electrolytes (for which *iR* drop is negligible), in the present system it is little higher, ranges from 0.5 to 0.9 V.

The specific capacitance of different carbon samples was calculated from galvanostatic charge/discharge cycling data of symmetrical devices assembled with two electrodes using the formula

$$C = \left[\frac{i(\mathrm{A}) \times t(\mathrm{s})}{W(\mathrm{g}) \times \Delta E(\mathrm{V})}\right] \quad (1)$$

where i is the discharge current, which is chosen as constant for all the samples as t is the discharge time, W, the mass of the active carbon material of the single electrode (working electrode), and ΔE the potential difference during discharge. The values of specific capacitance of different carbon samples were calculated for a specific current rate and plotted against cycle number as shown in Fig. 7. The specific capacitance values stabilize after 50 charge–discharge cycles and was sustained for over 1000 cycles. Among the three different carbons used, MB15 exhibits the higher specific capacitance of ~41 F/g even after 1000 cycles.

Obviously, such a high capacitance cannot be explained based on pure DLC formed at the interface of the low surface area carbons. That is, in addition to the current transient capacitive behavior of these graphite electrodes, the faradaic reaction (pseudocapacitance) was expected to occur due to insertion/extraction of Li^+. Therefore, the measured capacitance was not solely contributed by DLC but it includes pseudocapacitance (battery-like behavior) as well.

The stability of fabricated ECCs can be examined by conducting repeated charge–discharge cycling. A capacitor equipped with SFG6 carbon electrode was charged and discharged between 0 and 4.5 V at 6 mA/cm^2 to confirm the stability over repeated cycling. The variations of discharge capacitance (specific) versus cycle number are depicted in Fig. 8. The results show that the capacitor had stable (about ~41 F/g for MB15, ~35 F/g for SFG6 and ~33 F/g for KS6)

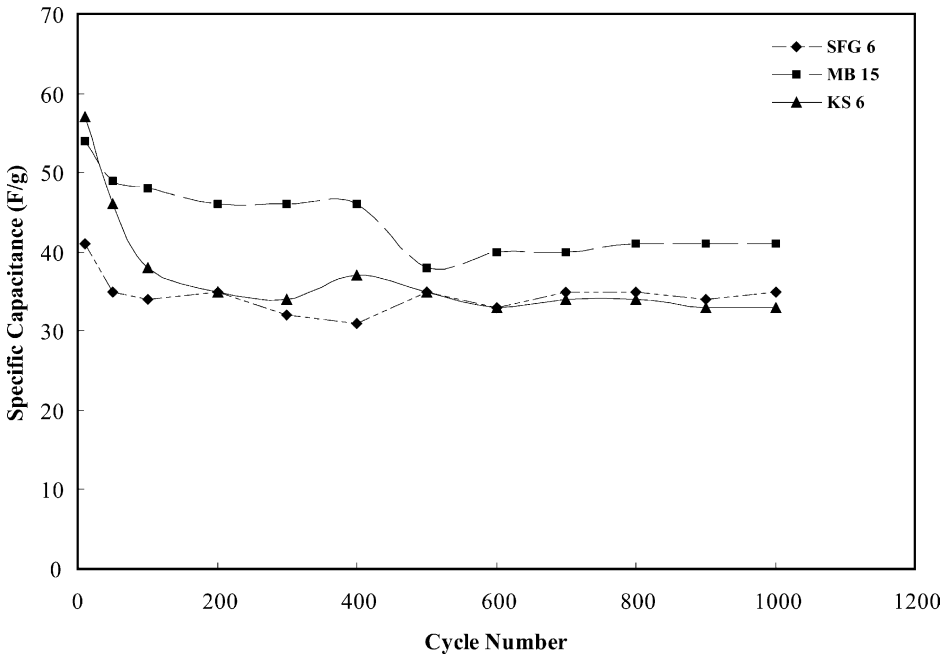

Fig. 8. Specific capacitance of three graphite samples as a function of cycle number.

capacitance and coulombic efficiency (80–90%) over 1000 cycles.

3.5. Ragone plots (specific power versus specific energy)

Ragone plot relates the specific power with the specific energy either for a constant current or power load and it is a better way to compare the performance of capacitors and batteries. To compare the performance of three graphites, the specific power and energy were calculated from the discharge curves of the ECCs at different current densities and they are plotted as shown in Fig. 9. Specific power (P) and specific energy (E) have been calculated according to the equations

$$P(\mathrm{W/kg}) = \frac{i(\mathrm{A}) \times V(\mathrm{V})}{m(\mathrm{kg})} \quad (2)$$

$$W(\mathrm{Wh/kg}) = \frac{i(\mathrm{A}) \times V(\mathrm{V}) \times t(\mathrm{h})}{m(\mathrm{kg})} \quad (3)$$

where i is the discharge current; V, voltage; t, time in hours; and m, mass of the cell excluding housing. In a symmetrical device configuration, the performance of SFG6 and KS6 was

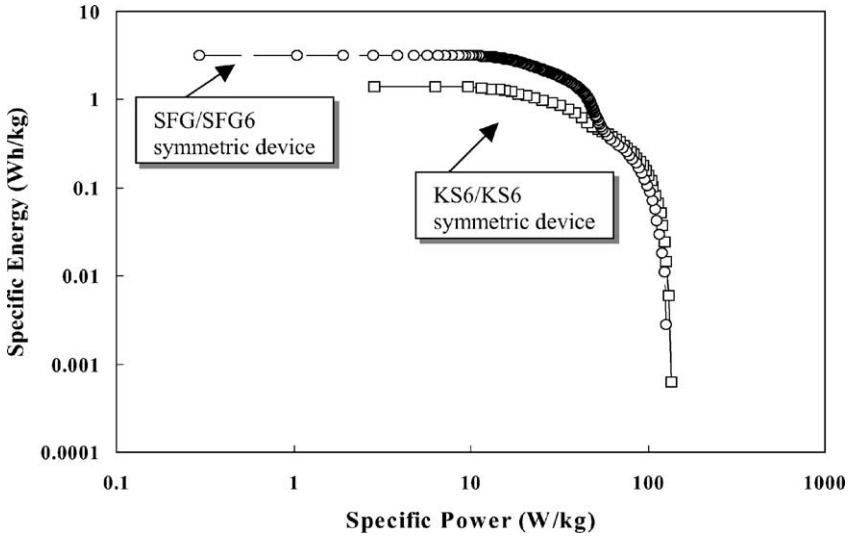

Fig. 9. Ragone plots of SFG6/SFG6 and KS6/KS6 symmetrical devices assembled in 1 M LiPF6/EC + DMC organic electrolyte. Celgard 2400 separator was used between the two carbon electrodes constituting the symmetrical electrode combination.

found to be better in terms of specific power, with a value of ∼1 kW/kg, as depicted in Fig. 9.

As for the dissimilar electrode configurations (asymmetrical device), SFG6/KS6 performs well with a specific power of ∼1.3 kW/kg.

4. Conclusions

In conclusion, we have successfully demonstrated high voltage electrochemical capacitors using low surface area graphite materials viz., KS6, SFG6, and MB15 (used as conductive additives in lithium-ion batteries) as electrodes and the performance of these graphites were studied and discussed in the light of both double layer capacitance and pseudocapacitance. Cyclic voltammetric studies revealed the faradiac reactions during the charge (anodic) process confirming that the high value of specific capacitance must have originated from some kind of pseudocapacitance which might be probably attributed to Li^+ insertion/deinsertion into graphitic layers of the graphites. Specific capacitance of up to 14.5 F/g was reached for a symmetrical device assembled with SFG6 graphite electrode.

At a low current rate (3 mA/cm^2), the specific capacitance of 63 F/g was achieved and the capacity decreased about 20% after 1000 cycles compared to the initial discharge process. Symmetrical devices assembled with two electrodes, for instance SFG6/SFG6 as well as KS6/KS6, offer higher specific power (135 W/kg) and specific energy (2 Wh/kg) due to their low *iR* drop. Thus, the conductive additive carbons used as electrodes in the present work demonstrated capacitor properties much better than conventional capacitors.

The important result is that we achieved a voltage window of >4 V, which is rather large, compared to the standard window of 2.5 V for ordinary electric double layer capacitors.

Acknowledgements

The work was partially supported by an MMU internal grant scheme.

References

[1] L. Bonnefoi, P. Simon, J.F. Fauvarque, C. Sarrazin, A. Dugast, J. Power Sources 79 (1999) 37.
[2] J.P. Ferraris, M.M. Eissa, I.D. Brotherston, D.C. Loveday, Chem. Mater. 10 (1998) 3528.
[3] B.M. Barnett, S.P. Wolsky, in: Proceedings of the 4th International Seminar on Double Layer Capacitors and Similar Energy Storage Devices, Florida Educational Seminar, Deerfield Beach, FL, 12–14 December 1994.
[4] A. Burke, J. Power Sources 91 (2000) 37.
[5] R. Kotz, M. Carlen, Electrochim. Acta 45 (2000) 2483.
[6] M. Ue, K. Ida, S. Mori, J. Electrochem. Soc. 141 (1994) 2989.
[7] T. Momma, X. Liu, T. Osaka, Y. Ushio, Y. Sawada, J. Power Sources 24 (1996) 253.
[8] A. Laforgue, P. Simon, C. Sarrazin, J.F. Fauvarque, J. Power sources 80 (1999) 142.
[9] C. Arbizzani, M. Mastragostino, L. Meneghello, Electrochim. Acta 41 (1996) 21.
[10] E. Naudin, N. Mehdi, C. Soucy, L. Breau, D. Belanger, Chem. Mater. 13 (2001) 634.
[11] B.E. Conway, J. Electrochem. Soc. 30 (1924) 508.
[12] B.E. Conway, V. Birss, J. Wojtowic, J. Power Sources 66 (1997) 1.
[13] A.D. Pasquier, I. Plitz, J. Gural, S. Menocal, G. Amatucci, J. Power Sources 113 (2003) 62.
[14] Y.U. Jeong, A. Manthiram, J. Electrochem. Soc. 149 (2002) A1419.
[15] D. Evans, in: Presented at the 9th seminar ECDL, deerfield Beach, FL, 1999.
[16] A. Yoshida, K. Nishida, S. Nonak, J. Nomoto, M. Ikeda, S. Ikuta, Japanese Patent 9-266143 (1997) (to Matsushita Electric).
[17] I. Tanahashi, A. Yoshida, A. Nihino, J. Electrochem. Soc. 137 (1990) 3052.
[18] S. Shiraishi, H. Kurihara, A. Oya, Carbon Sci. 1 (2001) 133.
[19] K. Naoi, Extended abstracts, in: Proceedings of the 49th Annual Meetings of the International Society of Electrochemistry, Kitaksshu, Japan, September 1998, p. 647.
[20] H. Probstle, C. Schmit, J. Fricke, in: Presented at the IAS6 Aerogel Conference, 2000.
[21] S.R.S. Prabaharan, T.Y. Tou, M. Begam, M.S. Michael, Solid State Ionics 152/153 (2002) 91.
[22] C.-H. Doh, H.-Soo Kim, S.-I. Moon, Carbon Sci. 1 (2001) 148.
[23] B.E. Conway, Electrochemical Supercapacitors, Kluwer Academic/Plenum publishers, New York, 1999, p. 1.
[24] M. Guo, P. Diao, R. Tong, J. Chin. Chem. Soc. (Taipei) 47 (2000) 1197.
[25] A.J. Bard, L.R. Faulkner, Electrochemical Methods Fundamentals and Applications, Wiley, NY, 1980, pp. 11–15.
[26] E.G. Gagnon, J. Electrochem. Soc. 120 (1973) 1052.